Sustainable Water Resources Management (2024) 10:173
https://doi.org/10.1007/s40899-024-01115-1

ORIGINAL ARTICLE

Reviewing early chemical weathering in the *Achala* Batholith (*Sierras Pampeanas*, Córdoba, Argentina)

P. J. Depetris[1]

Received: 18 April 2023 / Accepted: 23 May 2024

Abstract
Appraising weathering intensity and rate in areas subjected to a *weathering-limited* regime—i.e. *Achala* batholith (*Sierras Pampeanas de Córdoba*, Argentina)—is complicated due to regolith scarcity and the absence of soil profiles. The A-type granite exhibits characteristic landforms patchily mantled with coarse-grained (i.e. *grus*) and poorly sorted regolith in topographic lows. Physical weathering is substantial; chemical weathering of granite and derived debris is incipient. Rainfall and scarce snowfall carry continental chemical signatures due to aerosols, largely supplied by extensive neighboring playas and arid/semiarid environments. Initial assessments of *Achala*'s embryonic chemical weathering revealed that the chemical index of weathering (CIW) showed a significant difference between the granitic source and fine-grained regolith, triggered by mineral dissolution/hydrolysis. The $\delta^{18}O$ and $\delta^{2}H$ signatures of springs/streams are close to local rainfall, and show a significant deuterium excess (i.e. > 10 per mil). Stream chemistry suggested the contribution of plagioclase, and biotite, with calcite and gypsum (i.e. partly supplied as aerosols?), and likely pyrite oxidation adding to the dissolved pool. *PHREEEQC* inverse modeling applied in ephemeral/perennial springs, identified illite (~ 32 µmol kgw^{-1}), Ca-montmorillonite (~ 43 µmol kgw^{-1}), and sepiolite (~ 22 µmol kgw^{-1}) as main transferred phases. First-order streams broadly concurred with previous findings, with gibbsite (~ 23 µmol kgw^{-1}), chalcedony (~ 87 µmol kgw^{-1}), and kaolinite (~ 43 µmol kgw^{-1}) as frequent and more abundant crystalline phases. Modeling suggests that most dissolution and mineral formation occur within the realm of springs, with first-order streams largely expressing a reduced role in mole transferring.

Keywords Incipient weathering · Perennial/ephemeral springs · Mountainous streams · Weathering of granite · *PHREEQC* · Inverse modeling

Introduction

Thousands of scientific articles have addressed rock weathering in the evolution of modern Earth Sciences, and the one published in the Geological Magazine by GH Kinahan, over 150 years ago (Kinahan 1866), is among the early ones. Wedephol's (1995) and Nesbitt and Young's (1982) classic papers belong to the most cited group. It follows that many authors have dealt –and still do- with the subject matter, expanding the knowledge on the physicochemical characteristics and dynamics of weathering (e.g. Drever 2005, and references therein).

About fifteen percent of all the documents published on weathering have been devoted to probing into the mechanisms occurring in granites, in different climatic and tectonic settings (e.g. Oliva et al 2003; Lee et al. 2008; Vázquez et al. 2016; Kanamaru et al. 2018). Weathered in similar climates, different granite types would deliver contrasting water types. For example, a calc-alkaline granite would supply a dissolved weathering product that would differ from its alkaline counterpart, which is depleted in Ca^{2+}, and Mg^{2+}, and enriched in Na^{+} and SiO_2 concentrations (Meybeck 2005). Likewise, two geochemically similar granites in contrasting climates would also supply divergent water types. The literature on rock weathering is indeed abundant, and the one addressing the weathering of granites continues to attract scientific attention (e.g. Wang et al. 2023; Liu et al. 2024).

The articles focusing on the features and changing aspects of early weathering are a constrained subset among the thousands of papers generally dealing with weathering (e.g.

✉ P. J. Depetris
pedro.depetris@anc-argentina.org.ar

[1] Academia Nacional de Ciencias, Avenida Vélez Sarsfield 229–249, X5000WAA Córdoba, República Argentina

Published online: 13 September 2024

White 2005). Although it is not among the most cited papers, Garrels and Mackenzie (Drever 1997) published an article on the characteristics of early weathering (i.e. through the chemistry of springs and lakes) in the Sierra Nevada (California and Nevada, USA), seeking to relate major dissolved chemical components with the original minerals using an ingenious approach.

Several authors probed into the characteristics of weathering in the *Sierras Pamepanas* of Córdoba, Argentina, mainly in its two foremost mountain ranges: *Sierra Grande* and *Sierra de Comechingones* (e.g. Gaiero et al. 1998; Pasquini et al. 2002; Kirschbaum et al. 2005; Lecomte et al. 2005, 2009; García et al. 2007). The aim, here, is to review the characteristics of early chemical weathering in a uniform lithology scenario (i.e. aluminous A-type granite), controlled by weathering-limited denudation. This article revisits different approaches—mainly using previously published data -, succinctly comparing the characteristics of incipient weathering by probing into the chemistry of high-altitude (i.e. ~ 1100–2100 m a.s.l.) perennial/ephemeral springs and streams in the *Achala*[1] batholith (*Sierras Pampeanas*, Córdoba, Argentina).

Study area and methods

Geography and geology

Sierras Pampeanas designates a mountainous and partly semiarid region that occupies portions of seven Argentine provinces in central-west Argentina (~ 0.3 10^6 km^2). It comprises several mountain chains, generally following a north–south orientation, roughly parallel to the Andes. In this article, the attention will be placed on *Sierra Grande* and *Sierra de Comechingones*[2] (i.e. the northern and southern sectors, respectively), where the *Achala* batholith is a central element composed of a group of plutons with a mapped area of over 2500 km^2, thus constituting the largest group of intrusive rocks exposed in the *Sierras Pampeanas* (Fig. 1).

The *Sierra Grande* and *Sierra de Comechingones* belong in Argentina's Córdoba Province (i.e. *Sierras de Córdoba*). Jointly, they are ~ 490 km long and ~ 150 km wide. With a maximum altitude of 2884 m a.s.l., the *Cerro Champaquí*[3] is the highest peak in *Sierra de Comechingones*, whereas the *Cerro Los Gigantes* (2350 m a.s.l.) is the highest mountain in *Sierra Grande*.

The action of polar and subpolar fronts dominates climate in the area of interest. It lies in Argentina's temperate zone, exhibiting active atmospheric dynamics; the regional climate is typically continental, with irregularly distributed rainfall, which occurs mostly during (austral) summer and early autumn (e.g. Pasquini et al. 2006). About 75% of the total annual precipitation (i.e. historical regional mean ~ 1100 mm y^{-1}, record period 1943–2005, Martínez et al 2016) occurs between November and March. Mean monthly atmospheric precipitation in winter is ~ 40 mm (April-September), including occasional snowfall (e.g. Pasquini et al. 2006, and references therein). With considerable frequency, *Achala*'s highest ranges remain above the cloud level. They are thus subjected to 100% humidity (i.e. total cloud cover prevails 52% of the time, mainly during austral winter), thus water-feeding perennial/ephemeral springs (e.g. Pasquini et al. 2006).

The annual mean isotherm of ~ 16 °C encloses the area, falling to ~ 10 °C at 2000 m elevation. The maximum mean isotherm is ~ 20 °C, whereas in the higher areas, it is about ~ 14 °C. In contrast, the lowermost areas exhibit a minimum mean isotherm of ~ 9 °C whereas it is ~ 5 °C in the highest elevations. During winter, minimum temperatures can be − 10 ºC or lower (e.g. Pasquini et al. 2006, and references therein).

The analysis of recent rainfall and runoff data series from central Argentina has shown that there is, in general, a significant positive trend in rainfall, which has been verifiable since the second half of the twentieth century. Moreover, the spectral analysis also showed an apparent El Niño-Southern Oscillation (ENSO) limited influence south of ~ 31ºS (Pasquini et al. 2006).

Despite significant annual rainfall, it turns out that relatively steep slopes, and shallow regolith accumulations, yield scattered vegetation of grassland, and wide-ranging shrubbery. Morphological features typical of exposed granite, and gently undulating or relatively flat terrain are dominating features in the *Achala* batholith above ~ 1000 m elevation.

The *Achala* batholith (~ 31º07'S–32º00'S; ~ 64º30'W–65 º15'W) is a Devonian-Carboniferous granitic body (e.g. Lira and Sfragulla 2014). The U–Pb SHRIMP crystallization ages of the main monzogranitic facies (379 ± 4 Ma) and younger intrusive tonalites (369 ± 3 Ma) denote that the main central zone of the batholith is of Upper Devonian age (Rapela et al. 2008). Silica-rich monzogranites (70–74% SiO_2) are dominant although the batholith exhibits a wider SiO_2 range (60–76%), plotting inside the fields of the calc-alkaline to alkali-calcium series. They are aluminous A-type granites (i.e. peraluminous) and show characteristic enrichments in F, Ga, Nb, high Ga/Al, and low K/Rb ratios. Rapela et al. (2008) proposed that the *Achala* granites would represent

[1] From *achallay,* quechua for *nice, good-looking.*

[2] Common term used to designate the aboriginal inhabitants of the region (i.e. hênîa and kâmîare).

[3] "Water at the top" in the aboriginal language.

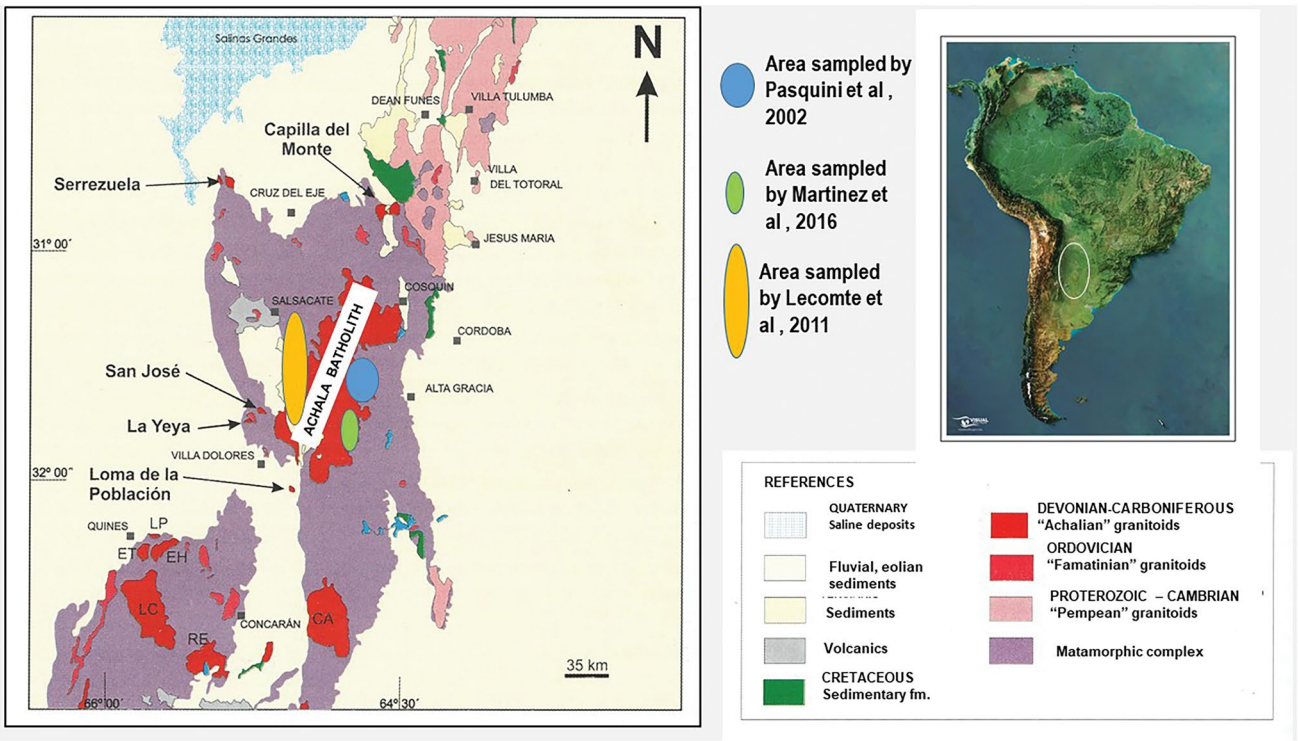

Fig. 1 Schematic geologic map of a sector of Argentina's *Sierras Pampeanas.* The *Achala* batholith ("*Batolito de Achala*"), with an area of ~ 2500 km.^{2}, is the central feature in the map, modified from Lira and Sfragulla (2014). The South American map (inset) shows the approximate location of the Sierras Pampeanas. The figure includes the sampled areas referred to in the text. The samples for stable isotopes were collected in the same area sampled by Pasquini et al (2002). The GNIP station (i.e. *La Suela*) is within the area sampled by Lecomte et al. (2011)

variable proportions of a juvenile mantle, with ε_{Nd} from -1.1 to -4.0, along with the inherited zircons.

The dominant lithofacies is a fractured porphyritic monzogranite. It is a holocrystalline rock composed of quartz, K-feldspar, plagioclase, white mica, and biotite. K-feldspar is present as large phenocrysts (~ 2 to 20 mm) set in a medium to the fine quartz-feldspar matrix. Zircon, apatite, rutile, and opaque minerals occur as accessory minerals, whereas clays, sericite, chlorite, and muscovite represent the secondary minerals set. Román-Ross et al. (1998) described a similar mineral assemblage, along with alteration products in the prevailing lithofacies. More recently, Lira and Sfragulla (2014) reviewed *Achala*'s Devonian-Carboniferous magmatism.

Methodology

The water chemical data, published elsewhere and relevant to this paper, is included in tables inserted in the text. All cited articles involving water chemistry used similar field (i.e. sample collection, filtration, conductivity, pH, and alkalinity titration), and analytical methodology (i.e. chemically suppressed ion chromatography with conductivity detection for anions, and ICP-MS for major cations and trace elements).

Using published data, the procedure proposed by Tardy (1971), and modified by Boeglin and Probst (1998), was initially used to probe into *Achala*'s weathering in first-order streams. With molar proportions, it involves the calculation:

$$RE = \left(3K^+ + 3Na^+ + 2Ca^{2+} + 1.25Mg^{2+} - SiO_2\right) / \left(0.5K^+ + 0.5Na^+ + Ca^{2+} + 0.75Mg^{2+}\right)$$

The coefficients in the above equation are contingent on the country rock's major primary minerals and correspond to typical granitic mineral composition, with micas and feldspars.

This paper includes previous unpublished data on stable isotopes (i.e. δ^2H, and $\delta^{18}O$). A sample set (i.e. seven samples) collected in the year 2000 was determined in *Achala*'s springs and streams. The samples were stored in 50 ml vials, tightly sealed without leaving air bubbles, and sent to Actlabs (Ancaster, Ontario, Canada) for subsequent analysis. Precision was 0.2 per mil for $\delta^{18}O$ and 3.0% for δ^2H. Vienna Standard Mean Ocean Water (VSMOW) was the standard selected for the analysis.

Campodonico et al. (2014) published the parent rock and regolith data recorded in a sample set collected in *Achala*'s batholith, describing the chemical and petrographic methodologies employed in their study. Using such data, a set of relative weathering indices (e.g. Price and Velbel 2003) was calculated to assess the chemical stripping exhibited by the mineral debris:

a) Chemical index of weathering {$CIW = (100)[Al_2O_3/(Al_2O_3 + CaO^* + Na_2O)]$};

b) Chemical index of alteration {$CIA = (100)[Al_2O_3/(Al_2O_3 + CaO^* + Na_2O + K_2O)]$};

c) Vogt's residual index [$V = (Al_2O_3 + K_2O)/(MgO + CaO^* + Na_2O)$];

d) Weathering index of Parker {$WIP = (100)[(2Na_2O/0.35) + (MgO/0.9) + (2K_2O/0.25) + (CaO^*/0.7 + Na_2O)]$; and,

e) Plagioclase index of alteration {$PIA = [(Al_2O_3—K_2O)/(Al_2O_3 + CaO^* + Na_2O—K_2O)]$}; CaO*is the CaO content included in the silicate fraction.[4]

The resulting geometric means were statistically evaluated. The *F* test was employed to assess the hypothesis H_0:$\sigma_1^2 = \sigma_2^2$ against the alternative H_1:$\sigma_1^2 \neq \sigma_2^2$. Similarly, the Student's *t*-test was used to test the hypothesis H_0:$\mu_1 = \mu_2$ against the alternative H_1:$\mu_1 \neq \mu 2$ (e.g. Davis 1986; Swan and Sandilands 1995). The comparison was between the source rock and the coarse- and fine-grained regolith.

The *Aqion*[5] software (i.e. version 7.3.3) was employed to revalidate the aqueous solutions, verifying occasional charge balance errors (CBE) and establishing full charge balance (i.e. CBE ≈ 0), if required, making small adjustments by using dissolved inorganic carbon (DIC) as the correcting parameter. The *Aqion* software was also used to calculate important chemical parameters (e.g. ionic strength, PCO_2, etc.).

PHREEQC Interactive (version 3.6.2.15100)[6] was the software employed to perform inverse modeling exercises, using rainfall data as the initial solution, and spring/stream chemical data as the evolved final solution (i.e. Table 9). The databases were those distributed with the program by the United States Geological Service (i.e. *wateq4f.dat, minteq.dat,* etc.), whereas the selected mineral phases are listed in the results (i.e. Table 10). All models ran with 0.025 (2.5%) uncertainties.

[4] The indirect method, proposed by McLennan (1993), involves the subtraction of P_2O_5 from the molar proportion of total CaO.

[5] https://www.aqion.de.

[6] https://www.usgs.gov/software/phreeqc-version-3.

Reviewing previous studies

Achala's regolith: main weathering features

Published research frequently approaches the assessment of weathering intensity and rate by contrasting the constituents of the fresh parent material with those of the weathered rock or the resulting unconsolidated mineral debris. This is a straightforward procedure in fully developed soil profiles (e.g. Krauskopf and Bird 1995; Drever 1997), usually found in transport-limited[7] denudation scenarios. Vázquez et al. (2016) provide a good example of transport-limited erosion in granitic rocks cropping out in the Coastal Range of central Chile. However, an indirect approach[8] is indicated when the composition of the parent material is not evident, as commonly happens in weathering-limited[9] denudation regimes. Such scenarios usually prevail in mountainous catchments, where regolith is thin or soils are poorly developed.[10] Relative methods are employed, therefore, to determine weathering intensity and rate (e.g. Bland and Rolls 1998). In such environment-type, primary-weathering reactions control stream chemistry, also markedly influenced by the chemistry of atmospheric precipitation.

The evaluation of rock weathering is a complicated case when occurring in a weathering-limited regime, even with uniform lithology. Mineral debris linked to an unmistakably identified provenance allows approaching the characteristics of weathering more truthfully, as it occurs with absolute methodologies. Weathering appraisal in a weathering-limited granite batholith is a good example, generally receiving significant attention.

The characteristics of Achala's regolith

The synergic action of physical, biological, and chemical weathering generates widespread *tors*,[11] *solution pits* and *pans*,[12] and *tafonis*, as dominant morphological features in a granitic landscape. Another important attribute

[7] Transport-limited denudation occurs where weathering processes are efficient at producing debris but where transport processes are inefficient at removing it (Carson and Kirkby 1972).

[8] Usually, the calculation of the ratio between the more stable and less stable oxides.

[9] Weathering- limited denudation occurs where erosion proceeds faster than debris-producing weathering (Carson and Kirkby 1972).

[10] High-energy mountain streams and rivers have been identified as singular river types, deserving focused attention (Wohl 2010).

[11] Isolated granite masses, consisting of either a single or of numerous combined blocks presenting variable degrees of angularity or roundness (Twidale 1968).

[12] Pits are small pockmarks (i.e. few millimeters to some centimeters in diameter and depth); pans develop from pits by lateral extension in all directions but for the most part maintain a perfectly flat floor (Fairbridge 1968).

Table 1 Mean composition of the country-rock and regolith in the Achala batholith (Basic data from Campodonico et al. 2014)

Components	Granite (N=4)	C-$G_{regolith}$ (N=3)	F-$G_{regolith}$ (N=5)
SiO_2	71.21±1.03	70.77±1.02	73.41±1.02
Al_2O_3	14.70±1.04	15.33±1.03	13.68±11.05
$Fe_2O_{3(Total)}$	2.22±1.32	1.87±1.36	1.63±1.34
MnO	0.04±1.10	0.03±1.39	0.02±1.22
MgO	0.58±1.32	0.44±1.43	0.31±1.37
CaO	1.01±1.33	0.99±1.25	0.72±1.13
Na_2O	2.75±1.10	2.85±1.09	2.66±1.06
K_2O	5.32±1.19	6.22±1.10	4.89±1.12
TiO_2	0.37±1.48	0.28±1.45	0.29±1.44
P_2O_5	0.26±1.23	0.22±1.10	0.11±1.19
LOI	0.89±1.21	0.91±1.26	1.62±1.60
Qtz[1)]	32.13±1.14	28.06±1.14	38.13±1.04
Kfs	31.84±1.20	37.01±1.20	29.54±1.11
Pl	27.14±1.13	27.87±1.13	25.96±1.08
Bt	3.76±1.32	3.02±1.31	2.49±1.36
Ms	2.95±1.19	2.48±1.19	2.83±1.36
Ap	0.57±1.23	0.48±1.23	0.23±1.18

[1)] CIPW norm (%); *C-G* Coarse-grained; F-G: Fine-grained

GM geometric mean, SD_G geometric standard deviation

is the patchy distribution of *grus* (i.e. the loose collection of weathered mineral grains) on the *Achala* batholith, on top of exposed rounded granite boulders (i.e. subjected to spheroidal weathering), or coarse regolith mixed with sand/silt grain-size detritus, accumulated in topographic lows, rock joints or edges. Campodonico et al. (2014) analyzed the characteristics of *Achala*'s regolith. Near the source rock, mineral debris is equivalent to the original granite, with grain size fluctuating between very coarse sand (~2 mm mean grain size) and silt (~62-µm mean grain size). Campodonico et al. (2014) supplied a detailed description of the dominant *grus*: abundant quartz (~1 to 5 mm), relatively unaltered K-feldspar grains (~0.5 to 11 mm), muscovite (~0.1 to 1.5 mm), and plagioclase (~0.1 to 1 mm) exhibiting an alteration comparable with the one verifiable in the outcropping monzogranite. Plagioclase shows alteration to sericite, clay minerals, and secondary muscovite. Likewise, biotite (~0.2 to 2 mm) exhibits minor alteration to chlorite and secondary muscovite.

The fine-grained mineral debris is composed of variable proportions of fine/very fine sand (250 to 62.5 µm), silt (62.5 to 3.9 µm), and clay (<3.9 µm). According to Campodonico et al. (2014), plagioclase (~0.2 to 2 mm) is more altered (i.e. virtually replaced by clays and sericite) than K-feldspar grains (~0.2 to 5 mm), which only show minor alteration. Fine-grained biotite (~0.2 to 0.7 mm) exhibits intense segregation of Fe-oxides. Inclusions in biotite, reported as accessory mineral phases, were apatite, rutile, zircon, and opaque minerals. The X-ray diffraction analysis of the <2 µm size-fraction showed clay mineral assemblages with illite > kaolinite > smectite, with traces of albite, K-feldspar, and quartz (Campodonico et al. 2014).

Table 1 shows the geometric means (GM) and the corresponding geometric standard deviations (SD_G)[13] of compositional data collected in the *Achala* batholith. Table 1 includes the granite's most frequent chemical composition, the CIPW-calculated normative mineralogy for the porphyritic monzogranite, and the coarse- and fine-grained regolith (Campodonico et al. 2014). Rapela et al. (2008), Lira and Sfragulla (2014), Campodonico et al. (2014), and references cited therein, supplied additional petrographic information on the *Achala* granite.

The cursory inspection of Table 1 shows slight differences between the chemical and mineralogical characteristics prevailing in the country rock (i.e. monzogranite) and the coarse- and fine-grained regolith. Campodonico et al. (2014) showed –using mass balance calculations- that there are no statistically significant chemical differences between granite and coarse-grained regolith. There were statistically significant losses of MgO, MnO, and P_2O_5 in the fine-grained regolith (i.e. concerning the unaltered granite), which Campodonico et al. (2014) ascribed to the early chemical weathering of biotite and apatite. Plagioclase alteration was apparent through petrographic observations. CIPW norm calculations (Table 1) supported these observations. Regolith sorting may be the cause behind other differences, like those of quartz or K-feldspar.

3.1.2 The REE signature of Achala's regolith. Geochemical research has shown that rare earth elements (REEs) are among the least mobile chemical elements in weathering. The variations in REE concentrations in natural waters have been explained by the presence of colloids that increase their apparent solubility (e.g. Gaillardet et al. 2005, and references therein). Different studies have determined that fractionation between light (LREE) and heavy REEs (HREE) is the outcome of variances in their affinity for being adsorbed onto surfaces. Accordingly, REEs are mobilized during weathering but are primarily recycled within the weathered environment rather than conveyed substantial distances in solution. This conclusion is important because it confirms the proposition that, for most weathering environments, REEs are transported by particles from the weathered milieu (e.g. Gaillardet et al. 2005, and references therein).

Achala's country rock-normalized spidergrams (Fig. 2) showed a discernible HREE enrichment, endorsed by the La_N/Yb_N ratios,[14] with the following geometric means

[13] When $a_1, a_2, \ldots a_n > 0$, GM = exp [1/n ln a_n]; likewise SD_G = exp {SD [ln (a_n)]}.

[14] N denotes normalization to mean granite composition.

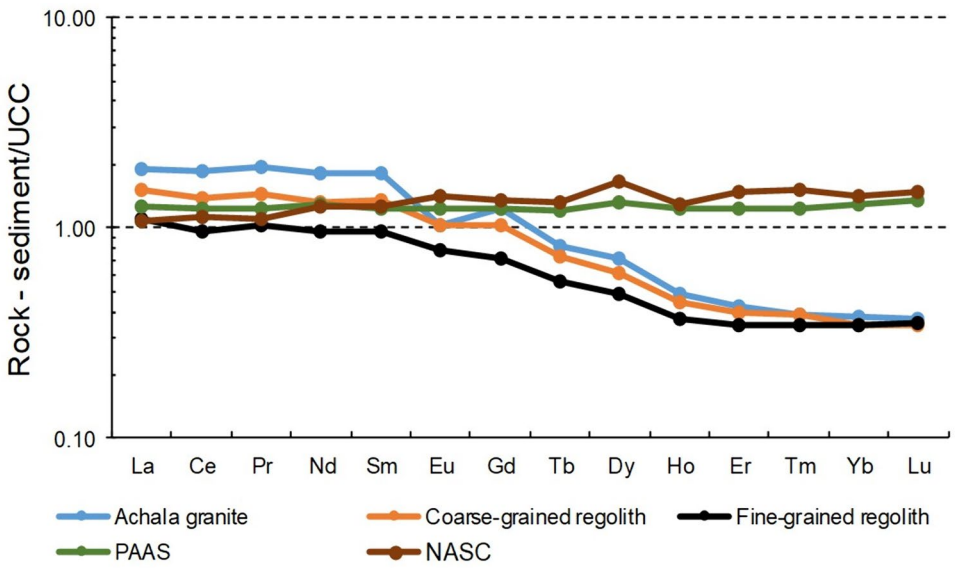

Fig. 2 Spider diagram (aka, spidergram) of UCC (Upper Continental Crust)-normalized REE concentrations in *Achala*'s granite, and regolith. North American Shale Composite (NASC) and Post Archean Australian Shale (PAAS) are included for comparison

Table 2 Arithimetic means and standard deviations for weathering índices applied in Achala batholith material

Weathering indices	Granite (N=4)	Coarse-grained regolith (N=3)	Fine-grained regolith (N=5)
CIW	70.2±3.34	70.7±1.93	70.9±0.48
CIA	54.9±1.11	53.9±0.64	55.6±1.58
Vogt ratio	2.7±0.50	3.0±0.50	3.0±0.29
WI	75.4±5.80	83.0±3.53	69.1±3.43
PIA	58.8±2.58	57.3±0.81	59.6±1.94

From data published by Campodonico et al. (2014)

Table 3 F and *t* statistics for the CIW index, testing *A chala* granite, coarse-(C-G), and fine– (F-G) grained regolith

F test[1)]				
		Granite (v=3)	C-G regolith (v=2)	F-G regolith (v=4)
Student's t-test[2)]	Granite		2.9833	**48.1086**
	C-G regolith	0.0800		**16.1257**
	F-G regolith	0.4713	0.0326	

[1)]Equality of variances; [2)]Equality of means

Bold numbers are significant ($p<0.01$)

(GM) ± geometric standard deviations (SD_G): 0.72 ± 1.112 for the coarse-grained regolith, and 0.54 ± 1.326, for the fine-grained regolith (Campodonico et al. 2014). Such previous study also showed Eu anomalies (i.e. Eu_N/Eu_N^*) in the coarse-grained regolith samples (GM ± SD_G: 1.40 ± 1.183), and in the fine-grained regolith (GM ± SD_G: 1.52 ± 1.075), which can be attributed to the retention of detrital feldspar in the coarse fraction (Campodonico et al. 2014).

The Upper Continental Crust (UCC)-normalized extended diagram (Fig. 2) shows that regolith—regardless of its dominant grain size—preserves a signature similar to the original granite, with LREEs dominating over HREEs. However, finer-grained-sized standards (e.g. wide-ranging provenance PAAS and NASC), show an enriched signature, with HREEs slightly richer than LREEs. Fu et al. 2019 have shown that A-type granites –as *Achala*'s- may have different REE enrichment situations in comparison with I- or S-type granites.

3.1.3 The assessment of weathering in Achala's granite using relative indices. The ratio between the more and the less stable oxides allows the assessment of weathering in rocks, sediments, or soils. This is the most frequent approach when the parent material is unknown or uncertain.[15] The result, expressed as an index, does not identify the minerals or minerals subjected to chemical stripping. The scientific literature describes several diverse weathering indices, most of which are based on the assumption that Al_2O_3 remains immobile during weathering (e.g. Price and Velbel 2003).

Several weathering indices for *Achala*'s country rock and the derived mineral debris are included in Table 2. A hasty inspection of each index's means and the corresponding standard deviations show small differences between the source rock and the coarse- (i.e. *grus*) or fine-grained mineral debris.

[15] The *Achala* batholith is subjected to a weathering-limited denudation regime and, hence, there are no fully-developed weathering profiles.

Table 4 Major physicochemical characteristics of perennial/ephemeral springs(p/e.s.) and related first-order streams draining granite in the *Achala* batholith Basic data from Pasquini et al. (2002)

Sample	Water temp.	Con-duct.	TDS[1)]	I. strength[1)]	pH	Cl^-	SO_4^{2-}	HCO_3^-	Ca2+	Na^+	K+	Mg^{2+}	Al	Fe	Si	CO_2 [1)]	DIC[1)]	TZ^+	P_{TOTAL}	$N\text{-}NO_3^-$	$N\text{-}NO_2^-$	$N\text{-}NH_3$
	°C	µS cm^{-1}	mg L^{-1}	µM		µM	µM	µM	µM	µM	µM	µM	µM	µM	µM	µM	µM	µeq L^{-1}	mg L^{-1}	mg L^{-1}	mg L^{-1}	mg L^{-1}
SG1-L (p/e.s.)	17.0	54.72	40.79	706.2	7.6	29.0	42.0	400.0	99.0	263.0	20.0	26.0	nd	nd	nd	23.80	411.50	533	0.017	0.480	0.002	0.100
SG4-L (p/e.s.)	15.8	23.09	15.16	302.4	8.3	2.0	21.0	100.0	53.0	69.0	1.0	15.0	nd	nd	nd	1.10	92.00	206	0.010	0.050	0.002	0.020
SG8-L (p/e.s.)	13.6	24.98	18.52	318.9	7.4	12.0	21.0	180.0	48.0	113.0	7.0	11.0	nd	nd	nd	18.46	194.39	238	0.003	0.006	0.003	0.070
SG11-L (p/e.s.)	12.3	46.96	35.53	579.6	7.3	25.0	21.0	320.0	85.0	217.0	12.0	25.0	0.778	1.379	340.39	42.70	359.70	449	0.003	0.060	0.004	0.090
SG12-L (p/e.s.)	10.0	49.98	38.81	618.7	7.4	27.0	5.0	380.0	95.0	241.0	16.0	22.0	0.222	0.304	258.85	41.80	414.50	491	0.013	0.050	0.003	0.050
G.M. (p/e.s.)		37.49	27.52	475.9	7.6	13.6	18.1	244.6	72.7	160.7	7.7	18.8	nd	nd	nd	15.39	255.89	351	0.007	0.053	0.003	0.058
SG2-L (stream)	12.9	31.59	19.99	384.3	7.4	15.0	31.0	7.0	52.0	131.0	10.0	15.0	nd	nd	nd	6.46	67.32	275	0.023	0.100	0.004	0.060
SG3-L (stream)	14.6	30.78	19.60	350.0	7.7	15.0	21.0	50.0	47.0	129.0	9.0	14.0	nd	nd	nd	2.05	41.87	260	0.013	0.140	0.002	0.070
SG5-L (stream)	17.5	56.22	40.10	754.4	7.6 21.0	15.0	73.0	350.0	113.0	181.0	30.0	45.0	nd	nd	nd	21.07	367.02	527	0.007	0.040	0.001	0.240
SG7-L (stream)	13.7	55.84	36.94	654.0	7.6	23.0	31.0	130.0	106.0	200.0	18.0	26.0	nd	nd	nd	7.34	119.51	482	0.020	0.250	0.002	0.090
SG2-L2 (stream)	9.9	30.95	20.45	390.8	7.7	18.0	16.0	150.0	51.0	155.0	6.0	13.0	0.927	0.215	252.80	6.85	127.67	289	0.033	0.060	0.003	0.010
SG7-L2 (stream)	10.5	42.50	24.11	544.0	8.8	24.0	21.0	150.0	67.0	210.0	8.0	17.0	1.001	0.448	306.92	0.33	76.20	386	0.070	0.100	0.004	0.050
SG10-L (stream)	9.8	96.25	74.11	1332.0	8.4	31.0	7.0	820.0	268.0	290.0	16.0	67.0	0.185	0.591	320.81	8.49	780.36	976	0.040	0.070	0.003	0.050
G.M (stream)		45.22	29.87	566.8	7.9	20.4	23.1	116.6	82.9	178.5	12.1	23.2	nd	nd	nd	4.53	137.70	403	0.023	0.093	0.002	0.058
Mean rainfall[1)2)]		8.08	4.82	96.0	6.7	17.0	11.0	8.0	8.0	21.0	10.0	7.0	nd	nd	nd	13.3	41.5	240	nd	nd	nd	nd

G.M.: Geometric mean; [1)]Calc. w/*Aqion* software; [2)]Lecomte et al. (2005); *nd* not determined

Fig. 3 Images of characteristic high-altitude (~1800 m a.s.l.) first-order streams in the *Achala* batholith. Notice water flowing over bare rock (left), and *tafoni* and *solution pans* (right), typical of the granitic scenario (Jennings 1968). Photographs are ~3 m wide

The resulting analysis showed that the null hypothesis had to be rejected when CIW (Harnois 1988) was used to compare the variances of fine-grained regolith with the source rock and with the coarse-grained regolith ($p < 0.01$) (Table 3). The remaining indices did not allow the rejection of the null hypotheses using the *F* test. The subsequent use of the Student's *t-test* (e.g. Davis 1986) in both rejected instances led to the additional conclusion that there is no evidence to suggest that the samples (i.e. granite, coarse- and fine-grained regolith) came from populations having different means (Table 3). Therefore, standard statistical methods showed that CIW was the only index in the chosen set, which, in terms of weathering, separated fine-grain regolith from granite and *grus*. Furthermore, it is worth noticing that CIW is the only index in the used set that does not include K_2O in the calculation.

Weathering in the Achala batholith: a brief overview of its dissolved chemical signature

Several authors have examined the dissolved geochemical characteristics of mountainous rivers draining the *Sierra Grande* and *Sierra de Comechingones* in Argentina's Córdoba Province. Lecomte et al. (2009), and Martínez et al. (2016), considered first-order streams in *Achala*[16] without fully exploring the linkage between the streams and the water-supplying springs. Both papers completed the respective investigations by probing through inverse modeling into the occurring weathering processes. On the other hand, Pasquini et al. (2002) studied the chemistry of *Achala*'s springs and first-order streams but did not use *PHREEQC* inverse modeling in the analysis. Such a procedure is presented in this article and the results are discussed in the following section.

Table 4 shows chemical data of a group of ephemeral-perennial springs and adjoining first-order streams draining a portion of *Achala*'s batholith (Pasquini et al. 2002). All streams are in the proximity of springs—although they do not necessarily have a direct connection with them—and they have a reduced interaction with fine-grained regolith, since most flow mainly in direct contact with bare granite (Fig. 3), often through rock fractures (e.g. temporary springs).

The streams exhibit a higher content of dissolved species than springs: springs belong to the *very dilute* water type (i.e. $TZ^+ \approx 350 \pm 40.8$ μeq L^{-1})[17] whereas streams are classified as *dilute* by a small margin (i.e. $TZ^+ \approx 400 \pm 118.7$ μeq L^{-1}). Ionic strength and, in general, other chemical variables (i.e. nutrients included), also show this difference. As expected, springs are more significant sources of dissolved inorganic carbon (DIC) than streams. Low-order streams (i.e. first-order, in particular) play an important role in the evasion of CO_2 from inland waters, a feature revealed during the assessments of the global carbon budget (e.g. Butman and Raymond 2011). The decreasing order of ionic abundance (i.e. $Na^+ > Ca^{2+} > Mg^{2+} > K^+$, for cations, and $HCO_3^- > Cl^- \geq SO_4^{2-}$ for negatively charged species) matches the sequence determined in *Achala*'s high-altitude

[16] Lecomte et al. (2009) expanded the investigation by probing into higher-order streams and rivers.

[17] $TZ^+ = 2Ca^{2+} + 2Mg^{2+} + Na^+ + K^+$.

Table 5 Major physicochemical characteristics of granitic first-order streams in the *Achala* batholith. Basic data from Lecomte et al. (2011)

Sample	Conduct.1)2) µScm-1	TDS2) mgL-1	pH	Temp. °C	Na+ µM	K+ µM	Ca2+ µM	Mg2+ µM	HCO3 - µeq L-1	Cl- µM	SO42- µM	Si µM	Fe µM	Al µM	TZ+ µeq L-1	DIC2) µM	CO22) µM
G1-LS	64.0	43.0	8.30	19.3	240	30	125	30	330	100	75	118	1.38	1.59	580	329	3.8
2G1-LS	32.5	20.4	6.65	8.7	123	10	60	15	90	40	60	153	9.56	9.34	280	199	78.7
3G1-LS	70.8	53.8	7.87	18.3	320	20	140	35	380	60	45	241	1.20	1.37	690	555	17.2
K7-PH	22.2	13.5	7.20	14.1	70	10	40	15	100	50	30	169	1.16	2.63	190	93	13.2
K8-PH	45.0	31.1	7.76	16.0	170	30	75	30	240	50	55	265	0.97	2.26	410	260	10.8
2K7-PH	53.9	36.5	6.41	9.7	310	20	60	20	70	110	55	200	2.22	7.78	490	569	299.1
2K8-PH	40.3	30.9	7.45	9.2	200	20	60	25	350	20	30	303	2.01	5.71	390	385	75.4
3K7-PH	24.6	16.8	6.30	21.0	70	20	50	15	70	30	25	128	0.59	3.04	220	304	163.6
3K8-PH	52.0	37.4	6.75	23.1	160	60	95	35	250	50	50	190	0.88	2.67	480	461	131.1
G18-MC	39.8	28.6	7.17	22.3	260	10	40	10	170	30	55	335	1.13	3.67	370	265	35.2
K22-MC	35.1	23.0	7.00	21.0	140	20	60	15	170	60	45	229	1.95	1.78	310	197	37.0
2G18-MC	27.0	19.5	7.13	13.4	190	3	25	5	170	30	30	327	0.77	2.96	250	195	32.0
2K22-MC	58.7	39.9	6.30	11.6	290	20	80	30	190	50	10	0 301	3.53	10.53	530	663	382.5
3G18-MC	30.2	20.4	6.66	19.1	180	10	30	10	150	30	50	182	0.77	3.15	270	213	73.3
3K22-MC	53.4	37.7	7.40	21.5	280	10	75	30	270	80	50	185	0.18	0.74	500	348	29.0
2K32-LR	54.7	41.4	6.90	8.2	200	30	95	55	460	30	40	291	0.45	0.85	530	575	155.3
3K32-LR	46.0	34.5	7.46	14.6	220	20	75	25	310	30	40	267	0.93	0.48	440	359	29.3

[1)]At 25 °C; [2)]Calc. w/*Aqion* software

Table 6 Major physicochemical characteristics of a granitic first-order stream (Sample site JA) in the *Achala* batholith. Basic data from Martínez et al. (2016)

Date	Conduct. µS cm^{-1}	TDS mg L^{-1}	pH	Na^+ µM	K^+ µM	Ca^{2+} µM	Mg^{2+} µM	Cl^- µM	SO_4^{2-} µM	HCO_3^- µeq L^{-1}	TZ^- µeq L^{-1}
March 2005	34.8	16.3	6.6	181	5.9	42.4	7.2	17.2	12.2	200.0	285.6
April 2005	37.2	18.6	7.8	187	4.3	47.4	7.0	19.2	12.6	261.9	300.1
May 2005	33.2	16.6	8.1	178	6.1	59.9	9.8	23.4	17.9	266.0	323.8
June 2005	48	24	6.4	191	9.0	62.4	11.3	28.8	13.3	282.7	347.4
July 2005	37.5	18.7	7.6	202	10.5	52.4	8.7	19.7	14.6	275.5	335.0
August 2005	38.4	19.2	6.6	232	11.0	74.9	10.5	17.8	13.6	278.0	414.1
December 2005	26.4	13.2	6.4	159	5.1	49.9	8.3	15.5	11.6	171.9	280.3
January 2006	25.9	12.9	7.1	172	5.1	49.9	7.7	19.2	10.9	213.9	292.1
February 2006	26.3	13.1	6.3	164	5.1	49.9	7.7	22.0	12.0	208.0	284.3
Sep.- Oct. 2001 - rain	n.d.	3.1	6.7	21	10.0	8.0	7.0	17.0	11.0	8.0	61.0

G.M.: Geometric mean; [1)]Calc. w/*Aqion* software; [2)]Lecomte et al. (2005); *nd* not determined

Table 7 Stable isotopes in springs and streams of the *Achala* batholith

Sample/type	δ^{18} O	δ D	D_e
SG1-L/spring	− 4.5	− 19	17.0
SG4-L/spring	− 6.3	− 36	14.4
SG11-L/spring	− 5.2	− 27	14.6
SG12-L/spring	− 4.9	− 24	15.2
SG2-L/stream	− 7.2	− 41	16.6
SG5-L/ stream	− 7.1	− 41	15.8
SG10-L/ stream	− 4.8	− 27	11.4

D_e= Deuterim excess; values in per mil

granite-draining streams (e.g. Lecomte et al. 2005, 2009; Martínez et al. 2016).

Lecomte et al. (2009) further probed into the physicochemical characteristics of chemical weathering occurring in the *Achala* batholith, showing the connection existing with geomorphological features. The data gathered in first-order order streams draining exposed granite was separated (Table 5) from the broader set -including higher-order streams- compiled by Lecomte et al. (2009). Contrasting with the preceding case, most first-order streams in the set drain areas have a substantial accumulation of fine-grained regolith and exhibit, therefore, an extended mineral–water contact.

Like in the preceding case, water in the high-altitude granite-dominated environment fluctuates between *very dilute* (i.e. which could be chemically close to atmospheric precipitations) and *dilute* chemical types ($185 < TZ^+ < 750$ µeq L^{-1}) (Table 5) (Lecomte et al. 2009). Following the chemical signature imposed by the country rock (Campodonico et al. 2014), the most frequent order of molar abundance among cations and anions was identical to the one determined in springs and streams (Pasquini et al. 2002).

Martínez et al. (2016) published a detailed study performed during a hydrological year in a small A-type granite-draining catchment in *Sierra de Comechingones*. The water chemistry determined in the first-order headwater was separated from the higher-order streams in the catchment, and the set is reproduced in Table 6. Mean $TZ^+ \approx 388 \pm 201.6$ µeqL^{-1} allowed its classification within the *dilute* water type, in agreement with the formerly described examples.

Results and discussion

Achala's atmospheric precipitations: the isotopic, and the Na+ /Cl– ratio signature

The chemical composition of atmospheric precipitation falling over a specific area may vary through time, with the distance from the oceanic source, and with anthropogenic/natural inputs, through aerosols. The water supplied by rain- or snowfall interacts with plants, regolith—or soil, if present -, and bedrock. Therefore, the geochemical attributes of water flowing in a drainage basin usually depend more on the flow paths followed by water through regolith and soils than on the chemical characteristics of atmospheric precipitation. However, exceptionally abundant rainfall events may result in riverine chemical signals that may be close, in chemical terms, to those exhibited by precipitation. Further, the dissolved chemical signal of mountainous streams draining catchments with scant regolith and/or immature soils may be more affected by precipitation chemistry than other river types, where prolonged and intimate contact with regolith/soils occurs (e.g. Meixner et al. 2000).

To probe with stable isotopes into the characteristics of *Achala*'s springs and rivers, $\delta^{18}O$ and δ^2H were determined

simultaneously with the sampling of other parameters (Table 7). An *excess* of ^{2}H (or D) relative to ^{18}O in the vapor is caused during evaporation by the diffusion of water molecules across a density gradient; the more diffusion (i.e. kinetic fractionation) that occurs, the higher the deuterium excess observed in vapor (i.e. evaporated moisture) (e.g. Bershaw 2018). The data shows that deuterium excess (D_e)[18] is significant (i.e. $D_e > 10$ per mil) in springs and streams of the *Achala* batholith. Such increased D_e in precipitation can arise from the important addition of re-evaporated moisture from continental sources to the water vapor traveling inland. Suppose moisture from precipitation with an average excess of 10 per mil is re-evaporated. In that case, the lighter $^{2}H^{1}H^{16}O$ molecule may again contribute preferentially to the isotopic composition of the water vapor, and this, in turn, leads to an enhanced deuterium excess in precipitation.

Figure 4 shows the $\delta^{18}O$ and $\delta^{2}H$ diagram. The Local Meteoric Water Line (LMWL) and the Global Meteoric Water Line (GMWL)were included for comparison. In addition to local springs and streams data, GNIP[19] isotope data for rainfall collected at nearby *La Suela* station (~ 31°S, ~ 64°W, 892 m a.s.l.) was included in the graph, showing that some rainfall events plot close to the isotopic signature of *Achala*'s springs and streams. Likely, chemical signatures in springs and first-order streams are significantly associated with the volume and intensity of atmospheric events.

The orthogonal regression for the LMWL (Fig. 4) has been calculated employing average weighted precipitation data (Dapeña 2008).[20] The plotted data shows that the $\delta^{18}O$ composition of springs appears somewhat less negative than the samples collected in first-order streams. Besides the significance of D_e described above, there is an aspect that must be underlined here, and it is that the sampled springs do not water-supply the sampled streams, being separated entities. A second relevant aspect is that springs are water-supplied by rainfall and winter-spring meltwater that is sometimes subjected to sublimation in the mountainous windy environment, thus affecting the isotopic composition. The third factor that likely impacts the isotopic signature of springs and streams is the frequent low cloud level (i.e. below 2000 m a.s.l.) that prevails in spring and autumn, frequently maintaining a water-saturated environment in the highest parts of the mountainous chain.

To probe into the geochemical linkage existing between atmospheric precipitations and first-order streams, Fig. 5

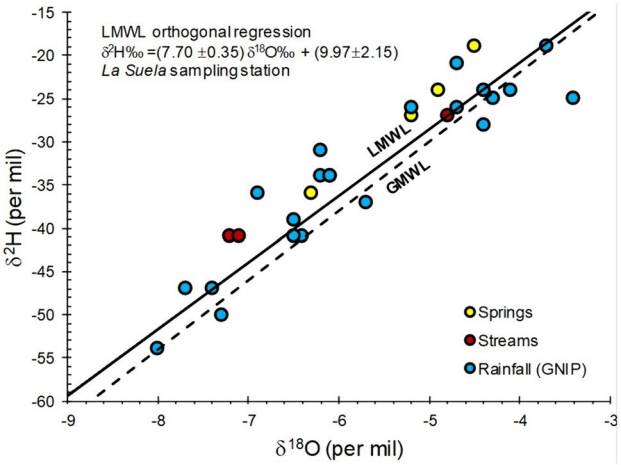

Fig. 4 Stable isotopes in springs, streams, and rainfall in *Achala*. Rainfall data from *La Suela* station [i.e. Global Network of Isotopes in Precipitation (GNIP)] was included for comparison. The Global Meteoric Water Line (GMWL) [$\delta^{2}H = 8\delta^{18}O + 10$], and the Local Meteoric Water Line (LMWL) [i.e. orthogonal regression equation included in the graph (Dapeña 2008) is plotted for reference]. The sampled streams are not hydrologically connected to the sampled springs. See text for additional information

shows a scatter diagram of Na^{+} vs. Cl^{-} concentrations, as determined in streams draining the *Achala* batholith. Only one sample plot within the field defined by Möller (1990) for continental rain (i.e. Na^{+}/Cl^{-}ratios between 1.1 and 1.8, not influenced by excess Na^{+} or Cl^{-}). The slope of the lines for other Na^{+}/Cl^{-} ratios of local rainfall (i.e.1.24, Lecomte et al. 2009), and the rainfall plus snowfall mean for the area (i.e. 2.0, Lecomte et al. 2009) are included for comparison.

Data suggests that there are two likely Na^{+} sources. One source is the aerosols from neighboring (i.e. to the N-NW of *Achala*, Fig. 1) salt flats/desert area, which supply allochthonous Na^{+} and Cl^{-}. Salty dust can be delivered by dominant northern winds (i.e. as dry fallout) or by rainfall/snowfall. Spring and stream data (Pasquini et al. 2002) in Fig. 5, further indicates that the weathering of Na^{+}-bearing minerals (e.g. plagioclase) is the additional likely source in springs for the Na^{+}excess.

The data plotted in Fig. 5 includes samples collected during the rainy (i.e. December-March) and dry (May–August) seasons in the pilot drainage basin (Martínez et al. 2016). Data implies that wet conditions (i.e. summer rains) promote the lowering of the Na^{+}/Cl^{-} ratio of local rainfall.

Observations on the chemistry of *Achala*'s springs and streams

The use of the *RE* parameter (Boeglin and Probst 1998) was the initial step to approach the nature of the likely weathering byproducts of silicate hydrolysis in *Achala*'s batholith. If

[18] $D_e = \delta D - 8\,\delta^{18}O$.

[19] IAEA/WMO (2020). Global Network of Isotopes in Precipitation. The GNIP Database. Accessible at: https://nucleus.iaea.org/wiser.

[20] https://bibliotecadigital.exactas.uba.ar/download/tesis/tesis_n4282_Dapena.pdf.

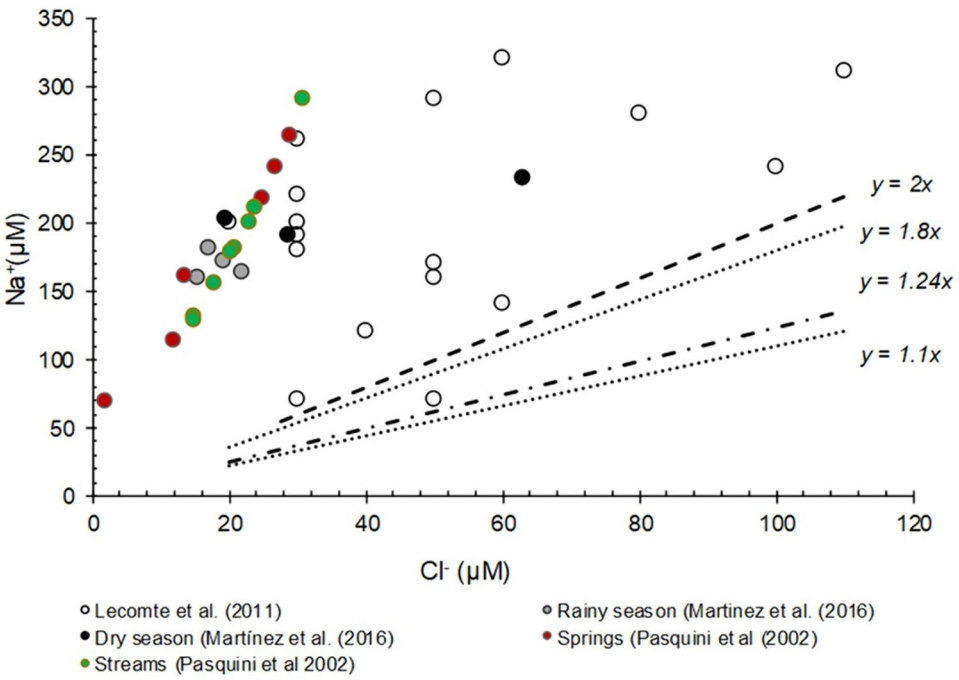

Fig. 5 Scatter diagram of Na^+ vs. Cl^- in first-order streams and springs draining the *Achala* batholith. The Na^+/Cl^- ratios (y/x = 1.1–1.8) are defined by Möller (1990). Local rainfall (y/x = 1.24), and the mean of local rainfall-snowfall (y/x = 2) are from Lecomte et al. (2005, 2009). Data from springs and first-order streams (Pasquini et al. 2002) show a considerable Na^+ enrichment. See text for further explanation

RE = ~ 0, the leading weathering product should be gibbsite; if *RE* = ~ 2, the formation of kaolinite should prevail, and if *RE* = ~ 4, smectite should be the most frequent solid weathering product (Boeglin and Probst 1998).

The data set in Table 5 shows a significant linear correlation (not shown, r = 0.67, $p < 0.001$) between conductivity (i.e. TDS) and *RE* (i.e.i.e..e., with values fluctuating in the ~ 1 to 3 range), suggesting that the likelihood of obtaining smectite as a weathering product in the early alteration of granite, increases with increasing TDS concentration. In some small first-order streams,[21] *RE* oscillates between ~ 0.4 and ~ 0.8, indicating the possible formation of $Al(OH)_3$(i.e. gibbsite), an essential building block in the structure of clays, like kaolinite and illite. The *RE* parameter applied to the data of Table 6 shows a tendency to produce gibbsite and kaolinite because *RE* fluctuates between ~ 0 and ~ 2.

Figure 6 shows the relationships between Ca^{2+}/Na^+ (x-axis), HCO^{3-}/Na^+, and Mg^{2+}/Na^+ (y-axes) (i.e. data from Tables 4, 5, and 6). Besides the theoretical calcite dissolution line, the other lines in Fig. 6 were plotted with data published by Garrels and Mackenzie (Drever 1997) in their reconstruction of source minerals and weathering products for Sierra Nevada ephemeral springs, and water with deeper circulation (Nevada and California, USA). Garrels and Mackenzie's model's weathering products included kaolinite and the dissolved pool. The reconstructed weathering reactions occurring in deeper water circulation included smectite and kaolinite as crystalline byproducts, and dissolved species, which exhibited higher concentrations than those determined in springs. Consequently, the evolution lines depicting deep water circulation were omitted in Fig. 6.

The somewhat wider scattering of Ca^{2+}/Na^+ vs HCO^{3-}/Na^+, associated with the y = 2 × line suggests a contribution of calcite dissolution, which appears to be mostly associated with streams in all cases (i.e. Pasquini et al. 2002, Lecomte et al. 2011, and Martínez et al. 2016). Precipitation as a byproduct of plagioclase hydrolysis, and dry fallout (i.e. wind-transported dust) are likely dominant sources in first-order streams. Conversely, alkalinity in springs seems associated with silicate hydrolysis, articulating with the possible mineral sources (i.e. biotite, apatite, and plagioclase) indicated by the analysis of weathered mineral debris (i.e. Sect. "Achala's regolith: main weathering features").

The variability of concentrations is significantly ampler in first-order streams than in springs. The source of Mg^{2+} seems consistently controlled by the hydrolysis of silicates in both, springs and streams.

The integral analysis of Fig. 6 shows that springs in *Achala*'s batholith are closer to temporary dynamics than to the deeper circulation of perennial springs (e.g. the Ca^{2+}/Na^+ molar ratio is ~ 0.6 in ephemeral springs and ~ 1.5 in the deeper circulation of the Sierra Nevada example.

Sulfate is a significant component among anions in the dissolved products of *Achala*'s early weathering. The geometric mean fluctuates significantly in granite draining waters: ~ 18.1 µM in springs, and 23.1 µM in streams (Table 4); ~ 46.3 µM (Table 5), and ~ 12.3 µM (Table 6). Sulfate in the mountainous springs and streams of *Achala*

[21] As defined by Strahler (1964).

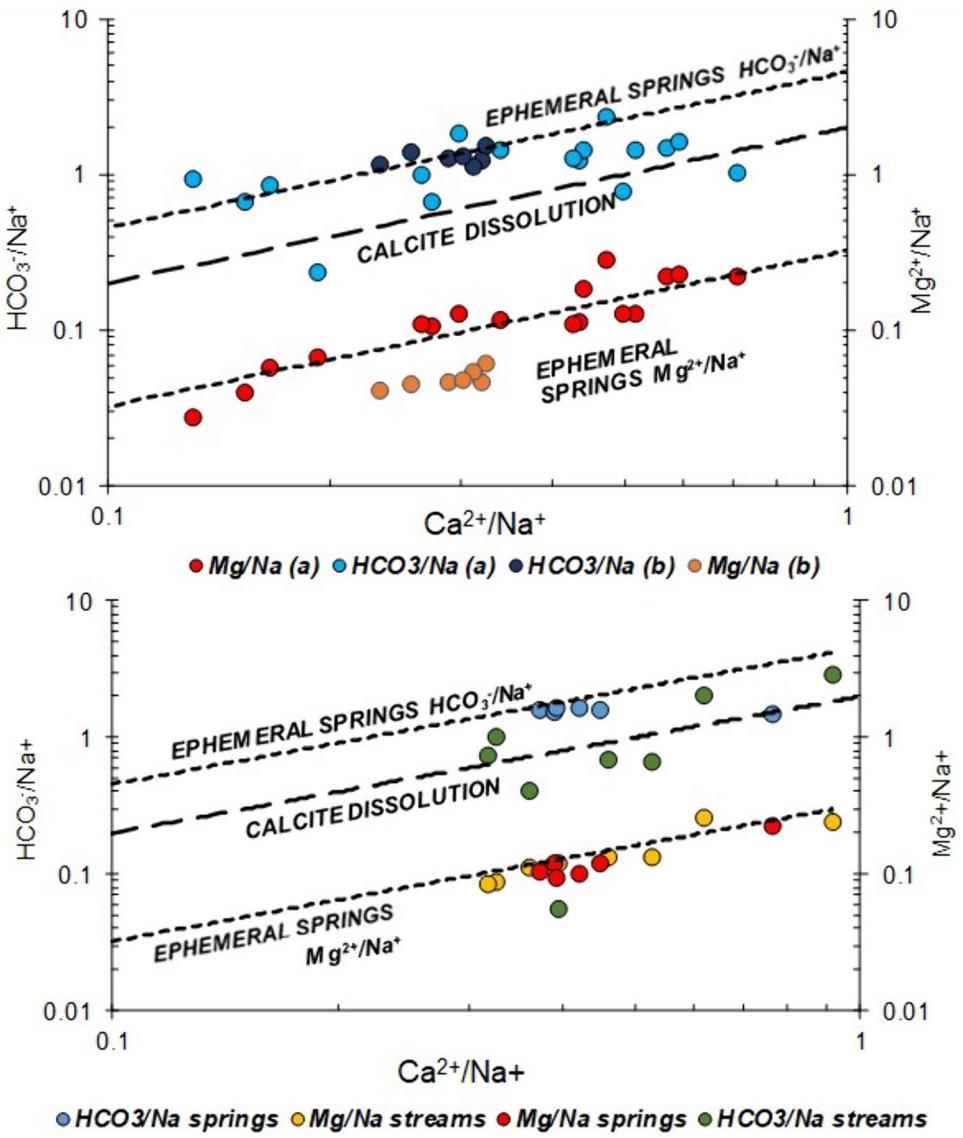

Fig. 6 Ca^{2+}/Na^{+} ratio plotted against Na^{+}-normalized HCO_3^{-} and Mg^{2+} in springs and first-order streams *Achala*'s batholith. Upper graph: First-order streams sampled by Lecomte et al. (2009)a, and by Martínez et al. (2016)b. Lower graph: springs and streams sampled by Pasquini et al. (2002). Plotted for comparison is the theoretical chemical evolution of calcite dissolution. The data to draw the chemical evolution of ephemeral springs (Sierra Nevada, USA) is from Garrels and Mackenzie (Drever 1982). Data from deep water circulation would be plotted outside the graph, to the right (e.g. Ca^{2+}/Na^{+} ratio ≈ 1.5). See text for additional explanation. Note logarithmic axes

is supplied either through the oxidation of sulfides or by dry fallout[22]/atmospheric precipitations. The maximum SO_4^{2-} concentration of sulfide oxidation in surface waters saturated with oxygen is ~ 200 µM (Tranter 2005).

Pyrite (FeS_2) is among the most common sulfide minerals on the Earth's surface, and it plays an important role in geochemistry and biological/environmental processes. When exposed to the atmosphere, pyrite oxidizes, forming sulfuric acid in the presence of humidity (e.g. Stumm and Morgan 1996)

$$FeS_2(s) + 7/2O_2 + H_2O = Fe^{2+} + 2SO_4^{2-} + 2H^{+}$$

Fe^{2+} endures oxygenation to Fe^{3+}, subsequently hydrolyzed to $Fe(OH)_3(s)$ liberating more acidity and coating mineral grains in the streambed. FeS_2 can reduce Fe^{3+}, pyrite oxidizes again, and releases more protons and Fe^{2+}:

$$FeS_2(s) + 14\,Fe^{3+} + 8H_2O = 15Fe^{2+} + 2SO_4^{2-} + 16\,H^{+}$$

The net effect of this system is the production of soluble iron (i.e. subsequently oxidized to Fe^{3+}), SO_4^{2-}, and acidity, which attacks calcite and other minerals. Thus, a substantial amount of Fe^{2+} is lost from the solution via the precipitation of $Fe(OH)_3(s)$ (Stumm and Morgan 1996). This mechanism can be inferred from Fig. 7, which also leads to the assumption that a considerable proportion of SO_4^{2-}, in *Achala*'s granite, is supplied by pyrite oxidation.

[22] Extended salt flats (*Salinas Grandes*), to the NE of the *Sierra Grande-Sierra de Comechingones* are significant sources of wind-blown halite, gypsum/anhydrite, and carbonate.

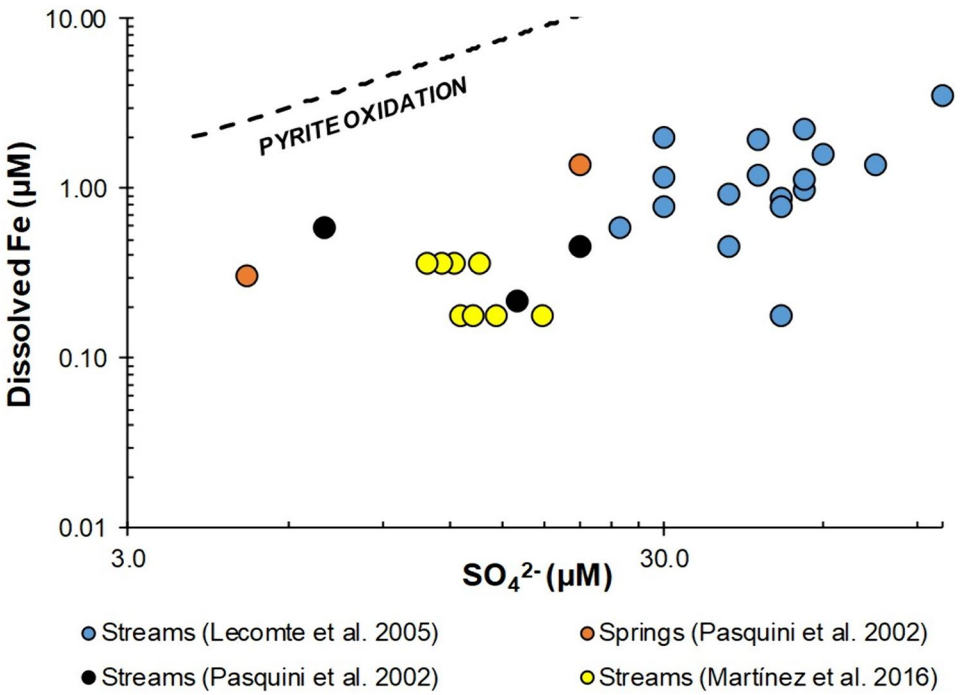

Fig. 7 Graph showing the relationship of SO_4^{2-} and Fe^{2+} in Achala's springs and first-order streams. The line depicts the theoretical dissolution pyrite line. A considerable proportion of Fe^{2+} is oxidized to Fe^{3+} and precipitated as $Fe(OH)^3$. See text. Note logarithmic axes

Exploring early weathering in springs/streams with *PHREEQC*.

PHREEQC is a computer program written in C programming language, conceived to execute varied aqueous geochemical calculations, and used to tackle an extensive variety of problems concerning water resources[23] (e.g. Parkhurst 1997; Parkhurst and Appelo 2013). The software is successfully used in exploring groundwater chemistry (e.g. Uliana and Sharp 2001) as well as probing into the dynamics of chemical reactions in the aqueous milieu (e.g. Marsac et al. 2011; Fu et al. 2019).

PHREEQC modeling seems more frequently used in connection with groundwater than in streams or rivers. However, the advantage of exploring the nature of weathering in a river catchment with a modeling approach is that it supplies a quantitative assessment of the ongoing hydrolysis/dissolution mechanisms, estimates the formation of new mineral phases, and allows a comparison with the traditional analytical approach.

PHREEQC inverse modeling was the tool used in the weathering assessment of *Achala*'s uppermost granite catchments (Lecomte et al. 2005, Martínez et al. 2018) (Table 8). In both instances, the starting solution was the mean regional rainfall chemical composition. The drainage basin modeled by Lecomte et al. (2005) covers an approximate area of 60 km^2 (i.e. fourth-order stream). In contrast, the catchment studied by Martínez et al. (2018) has an estimated drainage area of ~ 0.032 km^2 (i.e. first-order stream). A poorly sorted fine- and coarse-grained regolith mantles both drainage areas. Interstitial water had, in both instances, a significant residence time.

Both papers suggest the generation of similar precipitated weathering products (i.e. illite and kaolinite), although the smaller catchment produced more illite than kaolinite (i.e. ~ 160 against ~ 70 µmol kgw^{-1}) both, in absolute terms as well as in an area-normalized approach. The simulations failed to identify apatite as a likely reactant because the analytical data did not include phosphorous.

In contrast, the largest catchment produced more kaolinite than illite (i.e. ~ 106 against ~ 10-µmol kgw^{-1}) (Table 8). Hydrolysis seems more efficient in the smaller catchment, and reactions transfer more secondary minerals per unit area, probably due to higher PCO_2, and a significantly higher water residence time. Data was collected during (austral) wintertime (i.e. stream baseline flow) when solutes exhibited the highest concentrations.

Additional hydrochemical data (Table 4) was employed to model and compare weathering in the *Achala* batholith, by using chemical data collected in ephemeral/perennial springs and related first-order streams. The geometric means of the chemical data (Table 4) were used to develop *PHREEQC* inverse models, using mean rainfall data as a starting solution in both instances (i.e. in springs as well as in first-order streams) (Table 9).

The software supplied seven feasible models in each case (i.e. rainfall against springs, and rainfall against first-order streams). Table 10 shows the variability (i.e. as mol kgw^{-1})

[23] https://www.usgs.gov/software/phreeqc-version-3.

Table 8 Comparison of two *PHREEQC* inverse modeling exercises performed in contrasting granite (i.e., *Achala*) catchments

	Lecomte et al. 2005)[2)]		(Martínez et al. 2018)[3)]	
Phases transferred	Diss./Ppt.[1)] μmol kgw^{-1}	Diss./Ppt. μmol $kgw^{-1}km^{-2}$	Diss./Ppt. nmol kgw^{-1}	Diss./Ppt. μmol $kgw^{-1}km^{-2}$
CO_2 (g)	296	4.9	581.0	18.16
Biotite	8	0.1	15.5	0.48
Oligoclase	76	1.3	84.7	2.65
Calcite	23	0.4	3.9	0.12
Illite	**− 10**	**c0.17**	**− 164**	**− 5.12**
Kaolinite	**− 106**	**− 1.8**	**− 70.2**	**− 2.20**
Fluorite	nd	nd	10.5	0.33
Gypsum	nd	nd	0.4	0.01
K-mica	nd	nd	83.0	2.59
Halite	nd	nd	8.5	0.27
Total diss.	403	6.7	787.5	24.61
Total ppt.	**− 116**	**− 2.0**	**− 234.2**	**− 7.32**

[1)] Negative (bold) numbers are precipitated phases; *nd* not determined

[2)]~60 km^2, 4th order-stream; [3)] ~0.032 km^2, first-order stream

of the mole transferred for each dissolved or altered mineral phase as well as the number of models (i.e. out of the total possible models) where de indicated phase contributed to the reaction.

In both approaches (i.e. rainfall/springs, rainfall/streams) the most ubiquitous hydrolyzing/dissolving reactants were plagioclase, biotite, halite (i.e. rainfall), and CO_2 (g). Plagioclase was the most susceptible solid phase to dissolve (i.e. most frequent values ~ 89–97 μmol kgw^{-1}; ~ 28–30% of the total dissolved pool), reaching similar values in both, springs and streams, whereas CO_2 (g) was by far the most abundant phase, accounting for ~ 45 and ~ 48% of the dissolved pool in springs and first-order streams, respectively. Biotite was the second most abundant solid phase subjected to hydrolysis in both, springs and streams with ~ 2–3% of the total dissolved pool. Gypsum was a minor phase supplying Ca^{2+} and SO_4^{2-} in springs and streams and may be a proxy of pyrite oxidation in oxygenated environments. Other solute-supplying phases—with marginal frequency- in springs and streams were calcite, K-feldspar, and K-mica (Table 10).

Alternatively, the phases most frequently found (i.e. as likely alteration products) in both, springs and streams, were illite (~ 13 and ~ 8%, respectively, of the total pool) and gibbsite[24] (~ 24 and ~ 31%, respectively), with Ca-montmorillonite, kaolinite, chalcedony (i.e. *Achala* batholith's *tafoni* regularly exhibit silica speleothems within hollows), and sepiolite[25] as less frequent reactants.

Gibbsite and chalcedony (~ 24 and ~ 30%, with lower frequencies) lead in the set of resulting alteration species, with significant phase transferred in both, springs (~ 60-μmol kgw^{-1}) and streams (~ 90-μmol kgw^{-1}). Illite (mean ~ 31 μmol kgw^{-1}), and Ca-montmorillonite (mean ~ 43 μmol kgw^{-1}), appear to reach higher values in springs than in streams (illite mean ~ 23 μmol kgw^{-1}; Ca-montmorillonite mean ~ 34 μmol kgw^{-1}).

Both mean solutions (i.e. springs and first-order streams) evolved from a common starting solution (i.e. mean rainfall chemical composition). The differences between the starting solution (i.e. rainfall) and springs or first-order streams are assumed as caused by reactions between water, and the interacting minerals and gases. Therefore, *PHREEQC* modeling implies that most mole transfer (i.e. over 95%) occurs within the spring realm, establishing the chemical fingerprint found downstream, in first-order streams. The simulation of the reactions occurring between springs –as the starting solution- and 1st order streams—as a final solution- delivered only two models: one with gibbsite as the only phase (~ 60 to 70 μmol kgw^{-1}), and another with gibbsite (~ 60 μmol kgw^{-1})[26] along with sepiolite (~ 4.4 μmol kgw^{-1}), as likely transferred phases.

The results listed above are coherent with the information obtained from the *RE* equation, as well as with the exploration of chemical data, which denotes the occurrence of silicate hydrolysis -mostly in ephemeral springs -, along with pyrite oxidation, and calcite/gypsum dissolution.

[24] $Al(OH)_3$.

[25] $Mg_4Si_6O_{15}(OH)_2 \cdot 6H_2O$.

[26] Approximately equivalent to 78 μg $kgw.^{-1}$.

Table 9 Mean physicochemical characteristics of perennial/ephemeral springs(p/e.s.) and related first-order streams draining granite in the *Achala* batholith Basic data from Pasquini et al. (2002)

Sample	Water temp.	Con-duct.	TDS[1)]	I. strength[1)]	pH	Cl^-	$SO4^{2-}$	HCO_3^-	Ca^{2+}	Na^+	K^+	Mg^{2+}	Al	Fe	Si	$CO2^{1)}$	DIC[1)]	TZ^+	P_{TOTAL}	N-NO_3^-	N-NO_2^-	N-NH_3
	°C	µS cm-1	mg L-1	µM		µM	µM	µM	µM	µM	µM	µM	µM	µM	µM	µM	µM	µeq L^{-1}	mg L^{-1}	mg L^{-1}	mg L^{-1}	mg L^{-1}
G.M. (p/e.s.)	10.0–17.0	37.49	27.52	475.9	7.6	13.6	18.1	244.6	72.7	160.7	7.7	18.8	0.42	0.65	296.83	15.39	255.89	351	0.007	0.053	0.003	0.058
G.M (stream)	9.8–17.5	45.22	29.87	566.8	7.9	20.4	23.1	116.6	82.9	178.5	12.1	23.2	0.56	0.38	291.98	4.53	137.70	403	0.023	0.093	0.002	0.058
Mean rainfall[1)2)]	nd	8.08	4.82	96.0	6.7	17.0	11.0	8.0	8.0	21.0	10.0	7.0	nd	nd	nd	13.3	41. 5	240	nd	nd	nd	nd

G.M.: Geometric mean; [1)] Calc. w/*Aqion* software; [2)] Lecomte et al. (2005); nd: not determined

Summarizing and concluding comments

The *Achala* batholith is central Argentina's main peraluminous, A-type granitic core of the Sierras Pampeanas. This overview of its chemical weathering seeks to re-examine published and unpublished data, focusing on the early chemical weathering of large, silica-rich, granitic bodies. The mountainous region is subjected to a weathering-limited denudation regime (i.e. exposed mature weathering profiles are absent), revealing varied morphological features, typical of bare weathered granite. Abundant *grus* is ubiquitous on top of rounded and fractured boulders, and fine- and coarse-grained regolith has accumulated in topographic depressions.

Earlier published research and the approach followed in this contribution allow summarizing the following conclusions:

- Weathering indices did not disclose significant chemical differences between source rock and coarse- and fine-grained regolith (Campodonico et al. 2014; Martínez et al. 2018). A larger set of relative weathering indices (i.e. CIA, CIW, Vogt's residual index, WI, and PIA), basically concur with earlier findings, showing the nature of *Achala*'s chemical weathering. Due to the scant alteration of K-feldspar in the regolith, CIW is the only index that exhibits statistically verifiable geochemical differences between the fine-grained regolith, source rock, and *grus*.
- The regolith preserves the UCC-normalized REE spidergram of *Achala*'s batholith A-type granite. As the regolith's grain size decreases, so does the LREE/HREE fractionation, and the Eu anomaly. The outline of the coarse- and fine-grained regolith is markedly different from the pattern exhibited by standard mudstones (i.e. PAAS and NASC).
- Earlier papers (e.g. Lecomte et al. 2005, 2011; García et al. 2007; Martínez et al. 2018) reported chemical data on rainfall and snowfall falling over the *Sierras Grandes* of Córdoba (Argentina), which differs significantly from atmospheric precipitations with a distinct oceanic origin. Stable isotopes (i.e. $\delta^{18}O$ and δD) determined in *Achala*'s springs and streams are coherent with GNIP data, with important deuterium excess ($D_e > 10$ per mil), suggesting the significant addition of re-evaporated moisture from continental sources to the water vapor traveling inland. Frequent northern winds promote the effect of aerosols supplied by arid salt flats (i.e. situated to the N-NW of the *Sierras Pampeanas*), affecting the chemical quality of *Achala*'s stream water (e.g. García et al. 2022).
- The concentration of major ions conveys the image that the dominating mineral sources in springs, and low-

Table 10 Achala's batholith: *PHREEQC* inverse modeling of springs and streams. Models with the minimum number of phases. Uncertainties = 0.025 (2.5 per cent)

Phase mole transfers	Springs (perennial/ephemeral)			Streams (First-order)		
	Frequency (7 models)	Variability (μmol kgw^{-1})		Frequency (7 models)	Variability (μmol kgw^{-1})	
Plagioclase	7/7	82	96	7/7	88	106
Biotite	7/7	6	8	7/7	5	8
Halite	7/7	1	3	7/7	6	9
$H_2O(g)$	7/7	3.19E+07	3.37E+07	7/7	2.95E+07	3.38E+07
$CO_2(g)$	7/7	125	161	7/7	135	189
Gypsum	1/7	2	8	6/7	3	7
K-feldspar	1/7	29	32	1/7	13	33
Calcite	1/7	3	9	1/7	5	11
K-mica	1/7	29	40	1/7	13	33
Illite	6/7	**− 35**	**− 28**	4/7	**− 28**	**− 18**
Gibbsite	5/7	**− 66**	**− 52**	7/7	**− 102**	**− 80**
Ca-montmorillonite	2/7	**− 54**	**− 32**	1/7	**− 45**	**− 23**
Chalcedony	2/7	**− 70**	**− 50**	1/7	**− 108**	**− 66**
Kaolinite	1/7	**− 53**	**− 5**	1/7	**− 54**	**− 33**
Sepiolite	1/7	**− 26**	**− 18**	1/7	**− 21**	**− 8**
Total diss. [1)]		277	357		269	398
Total ppt.		**− 304**	**− 185**		**− 358**	**− 228**

Positive values are dissolved phases; negative values (bold characters) are precipitated phases; [1)] water not included

order streams are close to those denoted by the analysis of weathered mineral debris (Campodonico et al. 2014). The scattering in the plotting of Ca^{2+}/Na^{+} vs HCO^{3-}/Na^{+} or Mg^{2+}/Na^{+} implies significant variability in the rock-water contact (i.e. suggesting circulation through alluvium or rock fractures). Data points plotted next to the ideal calcite dissolution line suggest the contribution of disseminated calcite to the solute pool, partly supplied as wind-transported aerosols or as a plagioclase hydrolysis byproduct.

– Lecomte et al. (2005) led to the use of computer models (i.e. *PHREEQC*) to assess weathering intensity in the *Achala* batholith. Likewise, Martínez et al. (2018) evaluated exogenous processes in a small pilot catchment in the *Sierra de Comechingones.* Both approaches identified plagioclase, calcite, $CO_2(g)$, and biotite as the phases controlling the transfer of solutes. Martínez et al. (2018) also identified K-mica, fluorite, gypsum, and halite as subordinate reactants supplying solutes in a first-order granitic stream. Illite was the most abundant alteration product, followed by kaolinite. In contrast, such order was reversed in the fourth-order stream modeled by Lecomte et al. (2005), with far ampler and lengthy water-regolith contact. First-order streams appeared more efficient than the higher-order system in dissolving and supplying area-normalized mineral constituents (i.e. specific chemical yield decreases with increasing drained area).
– Pyrite oxidation was not included in simulations even though it is a probable source of SO_4^{2-} and total Fe as long as oxygenation remains operative. Iron is removed from the solution and coats mineral grains, immobilized as (oxy) hydroxides. Aerosol-supplied gypsum is a plausible additional source of SO_4^{2-} in streams, just as Fe is a likely derivative of pyrite oxidation and biotite hydrolysis.
– Data collected in ephemeral/perennial springs and associated streams draining the highest part of the *Sierra de Comechingones* (i.e. *Achala* batholith) (Pasquini et al. 2002) was employed to examine the geochemical characteristics of early weathering using *PHREEQC* inverse modeling. The models involved contrasting the mean chemistry of regional rainfall with the geometric means of the main chemical components of high-altitude springs and streams. Divergent from previous examples, water had a dominant contact with bare granite and lesser interaction with regolith in this scenario.
– Plagioclase, biotite, halite, and $CO_2(g)$ were the leading reactants in this instance. Less frequently identified, as likely phases delivering dissolved constituents, were K-feldspar, calcite, and K-mica. Gypsum reached a discernible frequency of occurrence in streams, herein

jointly interpreted as wind-supplied aerosols from neighboring playas, and as a proxy of pyrite oxidation.
- Contrasting with earlier findings, illite (in springs) and gibbsite (in streams), were recognized as the more ubiquitous mineral phases. Less frequently, *PHREEQC* identified Ca-montmorillonite and sepiolite as transferred phases in springs, whereas kaolinite and chalcedony played a similar role in low-order streams.
- This evaluation of early weathering in a granite batholith shows that inverse geochemical modeling applied in springs and streams may be a valuable addition when assessing weathering using a relative methodology in weathering-limited denudational regimes. It unveils mineral phases that likely participate as reactants or products in the process, which may be difficult to identify when exclusively investigating solid-weathered debris through instrumental methodologies. Mineral phases resulting from early weathering processes usually are in trace amounts and, hence, difficult to detect. Moreover, the exercise showed that rather than in low-order streams, most hydrolysis/dissolution takes place in springs (~95%) -whether ephemeral or perennial- as well as the transfer of mineral phases (~83%).

Author contributions Not applicable.

Funding The cited references identify funding sources. Field and analytical work performed in ephemeral/perennial springs and streams were supported by the *Universidad Nacional de Córdoba* (Córdoba, Argentina), and Argentina's *CONICET*.

Data availability Data is not deposited in a public repository.

Code availability Not applicable.

Declarations

Conflict of interest The author declares that he has no conflict of interest.

Ethics approval Not applicable.

Consent to participate Not applicable.

Consent for publication Not applicable.

References

Bershaw J (2018) Controls on deuterium excess across Asia. Geosciences 8, 257; https://doi.org/10.3390/geosciences8070257

Bland W, Rolls D (1998) Weathering. An introduction to the scientific principles. Arnold, London, 271 pp

Butman D, Raymond PA (2011) Significant efflux of carbon dioxide from streams and rivers in the United States; https://doi.org/10.1038/NGEO1294

Campodonico VA, Martínez JO, Verdecchia AI, Pasquini AI, Depetris PJ (2014) Weathering assessment in the Achala Batholith of the Sierra de Comechingones, Córdoba, central Argentina. I: Granite-regolith fractionation. Catena 123:121–134. https://doi.org/10.1016/j.catena.2014.07.016

Carson MA, Kirkby NJ (1972) Hillslope form and processes. Cambridge University Press, Cambridge

Dapeña C (2008 Light environmental isotopes: their application in hydrology and hydrogeology. Doctoral thesis, FCEN (Universidad de Buenos Aires). 442 pp (In Spanish)

Davis JC (1986) Statistics and data analysis in geology, 2nd edn. Wiley & Sons, New York, p 646

Drever JI (1982) The geochemistry of natural waters, 3rd edn. Prentice Hall, Upper Saddle River

Drever JI (1997) The geochemistry of natural waters. Surface and groundwater environments, 3rd edn. Prentice Hall, Upper Saddle River, p 436

Drever JI (2005) (Ed) Surface and ground water, weathering, and soils, Vol 5, Treatise on Geochemistry, Elsevier-Pergamon, Oxford, p 626

Fairbridge RW (1968) Solution pits and pans. In: Geomorphology. Encyclopedia of Earth Sciences. Springer, Berlin, Heidelberg. https://doi.org/10.1007/3-540-31060-6_342

Fu W, Li X, Feng Y, Feng M, Peng Z, Yu H, Lin H (2019) Chemical weathering of S-type granite and formation of Rare Element (REE)-rich regolith in South China- Critical control of lithology. Chem Geol 520:33–51

Gaiero DM, Pecsi HE, Depetris PJ (1998) Effects of quarry mining and other environmental impacts in mountainous drainage basins: the Chicama-Toctina example of Córdoba. Argentina Env Geol 34(2/3):159–216

García MG, Lecomte KL, Pasquini AI, Formica SM, Depetris PJ (2007) Sources of dissolved REE in mountainous streams draining granitic rocks, Sierras Pampeanas (Córdoba, Argentina). Geochim Cosmochim Acta 71:5355–5368

García MG, Lecomte KL, Depetris PJ (2022) Natural and anthropogenic sources of solutes in the wet precipitation of a densely populated city in Southern South America. Chemosphere. https://doi.org/10.1016/j.chemosphere.2021.132307

Harnois L (1988) The CIW index: a new Chemical Index of Weathering. Sediment Geol 55:319–322. https://doi.org/10.1086/648222

Jennings J.N. (1968) Tafonis. In: Geomorphology. Encyclopedia of Earth Science. Springer, Berlin, Heidelberg. https://doi.org/10.1007/3-540-31060-6_365

Kanamaru T, Suganuma Y, Oiwane H, Miura H, Miura M, Okuno J, Hayakawa H (2018) The weathering of granitic rocks in a Hyper-arid and hydrothermal environment: a case study from the Sør-Rondane mountains. Geomorphology 317:62–74

Kinahan GH (1866) The effect of weathering on rocks. Geol Mag 3(20):46–88

Kirschbaum A, Martínez E, Pettinari G, HeFerrero S (2005) Weathering profiles in granites, Sierra Norte (Córdoba, Argentina). Jour South Am Earth Sci 19:479–493

Krauskopf KB, Bird DK (1995) Introduction to geochemistry, 3rd edn. McGraw-Hill Inc, New York, p 647

Lecomte KL, Pasquini AI, Depetris PJ (2005) Weathering in a semiarid mountain river: Its assessment through PHREEQC inverse modeling. Aquatic Geochem 11:173–194

Lecomte KL, García MG, Fórmica SM, Depetris PJ (2009) Influence of geomorphological variables on mountainous stream water chemistry (Sierras Pampeanas, Córdoba, Argentina). Geomorphology 110:195–202

Lecomte KL, García MG, Fórmica SM, Depetris PJ (2011) Hydrochemistry of mountainous rivers (Sierras de Córdoba, Argentina): dissolved major elements. Lat Am Jour Sedim and Basin Anal 18:43–62

Lee SY, Kim SJ, Baik MH (2008) Chemical weathering of granite under acid rainfall environment, Korea. Environ Geol 55:853–862

Lira R, Sfragulla R (2014) The Devonian-Carboniferous magmatism: The Achala batholith and smaller plutons north of Cerro Champaquí. In Martino RD and Guereschi AB (ed) Geología y recursos naturales de la Provincia de Córdoba. Relatorio XIX Congreso Geológico Argentino, Tomo I, pp. 293–347 (In spanish)

Liu R, Chi Y, Xie Y, Kang C, Sun L, Wu P, Wei Z (2024) Characteristics and influencing factors of the granite weathering profile: A case study of a high latitude area in northern China. Minerals 14, 17. https://doi.org/10.3390/min14010017

Marsac R, Davranche M, Gruau G, Bouhnik-Le Coz M, Dia A (2011) An improved description of the interaction between rare earth elements and humic acids by modeling PHREEQC-Model IV coupling. Geochim Cosmochim Acta 75(19):5625–5637

Martínez JO, Campodonico VA, Fórmica SM, Depetris PJ (2016) Weathering assessment in the *Achala* Batholith of the *Sierra de Comechingones*, Central Argentina. II: Major hydrochemical characteristics and carbon dynamics. Environ Earth Sci 75:554. https://doi.org/10.1016/j.catena.2014.07.016

Martínez JO, Campodonico VA, Fórmica SM, Depetris PJ (2018) Weathering assessment in the Achala Batholith of the Sierra de Comechingones, Córdoba, Central Argentina. III: appraising chemical weathering. Env. Earth Sci 77:242. https://doi.org/10.1007/s12665-018-7417-3

McLennan SM (1993) Weathering and global denudation. J Geol 101:295–303

Meixner T, Bales RC, Williams DH, Campbell DH, Baron JS (2000) Stream chemistry modeling of two watersheds in the Front Range, Colorado. Water Resour Res 36:77–87

Meybeck M (2005) Global occurrence of major elements in rivers. In Drever JI (ed) Surface and ground water, weathering, and soils. Treatise on Geochemistry, Elsevier-Pergamon, Oxford, pp 207–223

Möller D (1990) The Na/Cl ratio in rainwater and the sea salt chloride cycle. Tellus 42B:254–262

Nesbitt HW, Young GM (1982) Early Proterozoic climates and plate motions inferred from major element chemistry of lutites. Nature 299(5885):715–717

Oliva P, Viers J, Dupré B (2003) Chemical weathering in granitic environments. Chem Geol 2002:225–256

Parkhurst DL (1997) Geochemical mole-balance modeling with uncertain data. Water Resour Res 33(8):1957–1970

Parkhurst DL, Appelo, CAJ (2013) Description of input and examples for PHREEQC version 3—a computer program for speciation, batch-reaction, one-dimensional transport, and inverse geochemical calculations: USGS Techniques and Methods, book 6, chap. A43, 497 p http://pubs.usgs.gov/tm/06/a43/

Pasquini AI, Lecomte KL, Piovano EL, Depetris PJ (2006) Recent rainfall and runoff variability in central Argentina. Quat Int 158:127–139

Pasquini AI, Grosso LB, Mangeaud AP, Depetris PJ (2002). Geochemistry of mountain rivers in the sierras Pampeanas: I. Spring and streams in the Achala Batholith, Córdoba province, Argentina. Rev Asoc Geol Arg 57(4):437–444 (In Spanish)

Price JR, Velbel MA (2003) Chemical weathering indices applied to weathering profiles developed on heterogeneous felsic metamorphic parent rocks. Chem Geol 202:397–416

Rapela CW, Baldo EG, Pankhurst RJ, Fanning CM (2008) The Devonian Achala batholith of the Sierras Pampeanas: F-rich, aluminous A-type granites. 6th South American Symposium on Isotope Geology, CD-ROM, 8p San Carlos de Bariloche, Argentina

Román-Ross MG, Kirschbaum AM, Ribeiro Guevara S, Arribere MA (1998) Weathering processes in the Achala Batholith, *Sierra Grande de Córdoba*: Chemical and mineralogical changes. Rev Asoc Geol Argen 54(4):480–488 (**(In Spanish)**)

Strahler AN (1964) Quantitative geomorphology of drainage basins and channel networks. In: Chow V (ed) Handbook of Applied Hydrology. McGraw Hill, New York, pp 439–476

Stumm W, Morgan JJ (1996) Aquatic chemistry. Chemical equilibria and rates in natural waters, 3rd edn. Wiley-Interscience, New York, p 1022

Swan ARH, Sandilands M (1995) Introduction to geological data analysis. Blackwell Science, Oxford, p 446

Tranter M. (2005) Geochemical weathering in glacial and proglacial environments. In Drever JI (ed) Surface and groundwater, weathering, and soils. Treatise on Geochemistry 5, Elsevier-Pergamon, Oxford, pp 189–205

Twidale CR (1968) Granite landforms. In: Geomorphology. Encyclopedia of Earth Science. 2Springer, Berlin, Heidelberg. https://doi.org/10.1007/3-540-31060-6_168

Uliana MM, Sharp JM Jr (2001) Tracing regional flow paths to major springs in Trans-Pecos Texas using geochemical data and geochemical models. Chem Geol 179:53–72

Vázquez M, Ramírez S, Morata D, Reich M, Braun J-J, Carretier S (2016) Regolith production and chemical weathering of granitic rocks in central Chile. Chem Geol 446:87–98

Wang W, Feng J, Qui M (2023) Mineral weathering and elemental migration in granite weathering pits (Gnammas): A case study in eastern China. Minerals 13:70. https://doi.org/10.3390/min13010070

Wedephol H (1995) The composition of the continental crust. Geochim Cosmochim Acta 59(7):1217–1232

White AF (2005) Natural weathering rates of silicate minerals. In Drever JI (ed) Surface and groundwater, weathering, and soils. Treatise on Geochemistry 5, Elsevier-Pergamon, Oxford, pp 133–168

Wohl W (2010) Mountain rivers revisited. American Geophysical Union, Washington DC, p 573